

# Construction of dynamic three-dimensional microstructure for the hydration of cement using 3D image registration

Lin Wang · Bo Yang · Ajith Abraham ·  
Lu Qi · Xiuyang Zhao · Zhenxiang Chen

Received: 20 June 2012 / Accepted: 5 April 2013  
© Springer-Verlag London 2013

**Abstract** Microstructure is one of the most important research issues in the field of cement hydration. The absence of imaging dynamic three-dimensional microstructure influences the investigation of cement hydration. Furthermore, it is impossible to confirm computer hydration models from real data perspective due to the lack of images of dynamic 3D microstructure. The evolution of the three-dimensional microstructure cannot be observed in situ easily. This article proposes an image registration-based approach to capture dynamic three-dimensional microstructure, whose original images are collected using microtomography. This is the first time that the dynamic 3D microstructure is imaged and analyzed for the hydration of cement. It allows imaging dynamic 3D microstructure for hydrating cement without using any extra equipment. Our research results indicate that the dynamic microstructure is captured easily with low cost and good precision.

**Keywords** Image registration · Microtomography · Cement hydration · Microstructure

---

L. Wang · B. Yang (✉) · L. Qi · X. Zhao · Z. Chen  
Shandong Provincial Key Laboratory of Network based  
Intelligent Computing, University of Jinan, Jinan 250022, China  
e-mail: yangbo@ujn.edu.cn

B. Yang  
School of Informatics, Linyi University, Linyi 276000, China

A. Abraham  
Machine Intelligence Research Labs (MIR Labs),  
Scientific Network for Innovation and Research, Auburn,  
Washington 98071, USA

A. Abraham  
IT4Innovations - Center of excellence, VSB - Technical  
University of Ostrava, Ostrava - Poruba, Czech Republic

## 1 Introduction

To improve the performance of cement and concrete, it is necessary to investigate the formation and evolution of cement paste. Therefore, the research of cement hydration is not only regarded highly for the theoretical understanding, but also for its practical significance and application prospects.

Microstructure is one of the most important issues in the cement hydration research field. The absence of dynamic 3D microstructure influences further investigation of cement hydration. Firstly, it will help scientists to investigate the formation and development mechanism of cement paste at the level of microstructure, e.g., the change of shape of air voids or the deformation of particles. Secondly, there are many established hydration models for the evolution of cement microstructure [1, 2], such as Hymo-Struc [3], CEMHYD3D [4], HydratiCA [5],  $\mu$ ic [6], etc. However, it is impossible to prove them from real data perspective. The dynamic 3D microstructure can help researchers to test and verify hydration simulation models from real microstructure perspective. Finally, the microstructure of cement paste is inhomogeneous in microscopic scale in practice and is lack of statistically representative. Therefore, large amounts of data are required to improve the representativeness. However, the cost, time, and image resolution result in the difficulty to collect large amounts of data. The dynamic 3D microstructure will also help us to analyze statistical parameters in the same region for the small data.

The evolution of the three-dimensional microstructure cannot be observed in situ easily. Although the three-dimensional information can be acquired by microtomography, it is hard to find accurately the same position of cement paste viewed at different ages without extra

equipment, especially when the specimen is cured outside the equipment.

The difficulties faced in acquiring images of dynamic three-dimensional microstructure and the progress achieved by image registration techniques inspire us to explore building dynamic three-dimensional images for the microstructure of hydrating cement paste using image registration.

This paper makes the following major contributions:

- An image registration-based approach is proposed to image dynamic microstructure with low cost and good precision.
- This is the first time that the dynamic three-dimensional microstructure is imaged and analyzed for the hydration of cement.
- Several dynamic microstructures are captured and investigated.

Rest of the paper is arranged as follows. Section 2 outlines the background and related works. Section 3 explains the proposed image registration-based method in detail. Section 4 outlines and discusses the experimental results followed by conclusions in Sect. 5.

## 2 Background and related works

Investigating microstructure is one of the most important issues in the research of cement hydration. Nowadays, there are several equipments for the observation of cement microstructure, such as scanning electron microscope (SEM), scanning transmission electron microscopy (STEM) and microtomography ( $\mu$ CT) [7–9]. The SEM, which has been widely used in cement research, has a great ability in observing surface morphology and formation of minerals, investigating effects of admixtures, determining durability problems and service life, improving the ability to characterize the microstructure of cement paste [11]. Despite the high resolution and fine clarity of image, only two-dimensional information can be imaged by SEM, which limits the scope of the application in the three-dimensional world.

Since microtomography operates on the same basic principles as medical computed tomography scanners, it provides the three-dimensional images from finite radiological images; but with much higher spatial resolution. Besides the access to the third dimension, the interest of microtomography, compared with SEM, is that no prior preparation of the paste-drying, resin impregnation and polishing are needed. Therefore, any possible artifacts are avoided. Bentz et al. [7] collected 3D data sets using the microtomography in European Synchrotron Radiation Facility. Most of the images are for hydrating Portland

cement pastes. Gallucci et al. [8] studied cement pastes aged from 1 to 60 days using synchrotron microtomography on the MS-X04SA beam line at the Swiss Light Source. Promentilla et al. [9] investigated the microstructure of cement-based materials using microtomography technique, including microfocus and synchrotron. Pourchez et al. [10] evaluate and compare the impact of cellulose ethers on water transport and porous structure of cement-based materials in both fresh and hardened state. The 3D porous media of samples are investigated using synchrotron radiation X-ray microtomography.

To better understand the correlation between microstructure's development of cement paste and cement behavior during setting, dynamic in situ observations on cement pastes have been conducted. Giri Venkateela et al. [12] conducted in situ observations on microstructure development of fresh pastes on three different cement pastes by using an extra equipment Quantomix WET-SEM<sup>TM</sup> capsuling system in a conventional SEM. Pourchez et al. [10] performed fast X-ray microtomography scans to show dynamic of cement microstructure in fresh state during the first hour of hydration. The evolution of three-dimensional microstructure cannot be observed using SEM. Further, although the three-dimensional information can be acquired by microtomography, it is hard to find the accurate same position of cement paste viewed at different ages, especially when curing specimen outside the equipment.

The question that arises here is whether we can image dynamic three-dimensional microstructure (four-dimensional) with simplicity, low cost and good precision?

Image registration has opened new feasibilities for solving this problem without using any extra equipment. It is the process of transforming different sets of data into one coordinate system. Data may be multiple photographs, data from different sensors, from different times, or from different viewpoints. The image registration procedure can be divided into four basic steps: feature detection, feature matching, mapping function design, and image transformation and resampling [13]. This technology has been widely used in various fields, such as biology, medicine and remote sensing. Fowlkes et al. [14] described a registration technique that takes image-based data from hundreds of *Drosophila* blastoderm embryos, for a reference gene and one of a set of genes of interest, and built a model VirtualEmbryo. Tomer et al. [15] obtained a high-resolution gene expression map for the developing annelid brain using a newly developed protocol for cellular profiling by image registration. Grunwald [16] developed a super-registration approach using fluorescence microscopy that can overcome the current limitations of co-localization by means of measuring intermolecular distances of chromatographically different fluorescent molecules with nanometer

precision. Wong et al. [17] presented an automatic registration system built to register satellite and aerial remotely sensed images.

The difficulties faced by acquiring dynamic three-dimensional microstructure and the progress achieved by image registration techniques inspire us to explore building dynamic three-dimensional images for the microstructure of hydrating cement paste from microtomography data using image registration.

### 3 Method

#### 3.1 Specimen preparation

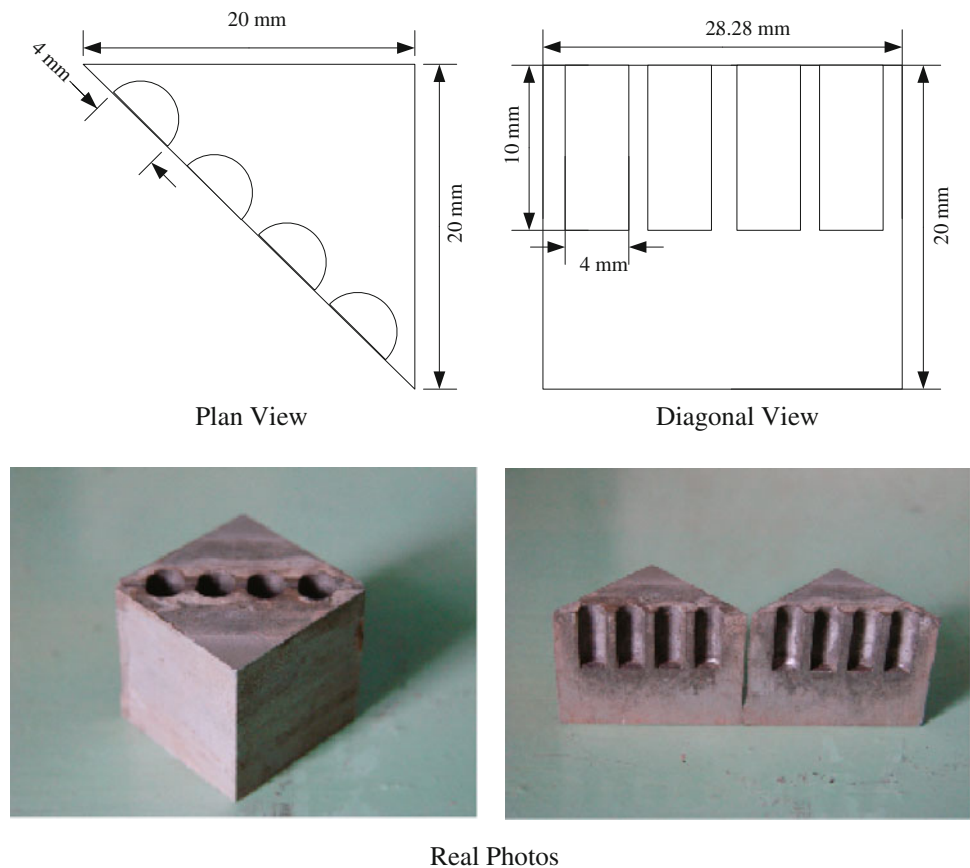
The determination of geometry of shape and size of cement specimen affects the scanning results because the full scan field for CT is a cylinder and the most efficient shape to scan is also a cylinder [18]. Therefore, a couple of aluminum molds (shown in Fig. 1) are customized to prepare cement specimen. To ensure the prepared specimen fits inside the field of view and does not move during the scan, the diameter is set to 4 mm, which is based on repeated comparisons and scanning, to observe the microstructure as large as possible. On one hand, the extracted

microstructure from smaller cylinder may suffer lack of representativeness, especially when the edge is  $<200 \mu\text{m}$  [8]. Since the air void diameter can be larger than  $500 \mu\text{m}$  [9], it is hoped to enlarge the size of specimen to reduce influence from rare huge voids on the representativeness of microstructure. Further, it is difficult to control the homogeneity and water-to-cement ratio in the fine specimen [8]. It is also difficult to find the same part (roughly) in the fine specimen during acquisition. On the other hand, if the diameter is larger than 4 mm, we have to increase the X-ray energy to penetrate cement specimen. However, different minerals cannot be distinguished clearly at high energy [18].

#### 3.2 Image acquisition

The prepared specimens are scanned at different ages using microtomography (Fig. 2). Then, the 3D images are reconstructed from X-ray projection images. However, as beam-hardening and ring artifacts influence the gray levels in the reconstructed images, quantitative analysis becomes a major problem. The beam-hardening artifact was corrected by polynomial beam-hardening correction [19]. Ring artifact was reduced by the method proposed by Sijbers and Postnov [20].

**Fig. 1** Specimen mold for cement paste



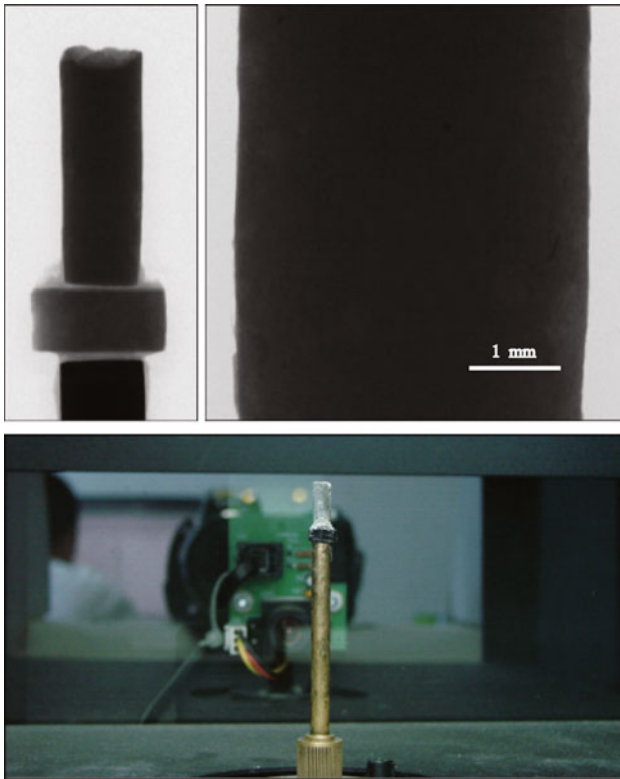


**Fig. 2** Specimen scanning: panoramic X-ray projection image (top-left); X-ray projection image (top-right); original photo of scanning specimen (bottom)

### 3.3 Three-dimensional registration

Based on the collected three-dimensional data, the image of dynamic microstructure of cement specimen can be built by three-dimensional registration from the images of the same specimen viewed at different ages. The purpose of image registration [13] is to find a transformation  $T$  within the class of transformations  $E$  between a reference image  $I$  and a floating image  $J$  according to a similarity criterion  $C$

$$\hat{T} = \operatorname{argmax}_{T \in E} C(I, T(J)) \quad (1)$$

Selecting reference cement image follows two rules: the image at the age that is not out of the field of view and located in the center as much as possible. Taking microstructure at one age as reference image, and at other ages as floating image, Fig. 3 depicts the general process of cement three-dimensional registration. At first, the floating cement image is rigid transformed to new position according to six degrees of freedom. Then, gray information is assign to the new image lattice using nearest neighbor interpolation. Finally, the similarity between the new floating image and reference image is measured to evaluate the effect of these degrees of freedom. The above

procedure is repeated using some optimization method until finding the best combination of degrees of freedom and corresponding accurate registered image.

#### 3.3.1 Transformation

Since the size and shape of full cement cylinder will not accompany distinct deformation during hydration when it is cured in water, the cement cylinder can be deemed as a rigid body. Then, the spatial transformation between cement specimens at different ages is a rigid transformation. There are six degrees of freedom set in a three-dimensional rigid transformation:

- Translation along the  $x$  axis  $t_x$
- Translation along the  $y$  axis  $t_y$
- Translation along the  $z$  axis  $t_z$
- Rotate around  $x$  axis  $\theta_x$
- Rotate around  $y$  axis  $\theta_y$
- Rotate around  $z$  axis  $\theta_z$ .

Rigid transformation matrix of a point  $(x, y, z)$  in cement cylinder from original position to transformed position is shown in Eq. (2).

$$\begin{bmatrix} x' \\ y' \\ z' \\ 1 \end{bmatrix} = \begin{bmatrix} R_{11} & R_{12} & R_{13} & t_x \\ R_{21} & R_{22} & R_{23} & t_y \\ R_{31} & R_{32} & R_{33} & t_z \\ 0 & 0 & 0 & 1 \end{bmatrix} \begin{bmatrix} x \\ y \\ z \\ 1 \end{bmatrix} \quad (2)$$

where  $R_{11} = \cos \theta_y \cos \theta_z$ ,  $R_{12} = \cos \theta_x \sin \theta_z + \sin \theta_x \sin \theta_y \cos \theta_z$ ,  $R_{13} = \sin \theta_x \sin \theta_z - \cos \theta_x \sin \theta_y \cos \theta_z$ ,  $R_{21} = -\cos \theta_y \sin \theta_z$ ,  $R_{22} = \cos \theta_x \cos \theta_z - \sin \theta_x \sin \theta_y \sin \theta_z$ ,  $R_{23} = \sin \theta_x \cos \theta_z + \cos \theta_x \sin \theta_y \sin \theta_z$ ,  $R_{31} = \sin \theta_y$ ,  $R_{32} = -\sin \theta_x \cos \theta_y$ ,  $R_{33} = \cos \theta_x \cos \theta_y$ . The abridged general view of rigid transformation for cement cylinder is shown in Fig. 4.

#### 3.3.2 Interpolation

As the forward transformation is complicated to implement and can produce holes and/or overlaps in the output image [13], the backward transformation using image interpolation is chosen in this research. When points of original image are transformed using rigid transformation, new coordinates of points may not be an integer. Therefore, gray information of these points can be imaged using interpolation method.

The gray value in a voxel reflects the mineral information. So, the change of gray value will affect the discriminating mineral and overall distribution of gray value. The other interpolation method, such as Bilinear and Bicubic interpolation, is not suitable for cement registration because they calculate a new estimate value for a voxel and blur the resultant images. Therefore, we adopt nearest

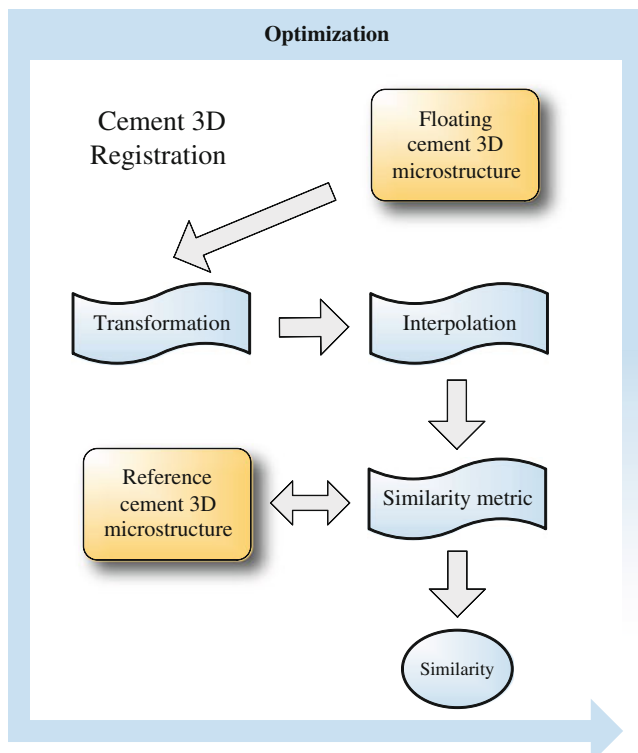


Fig. 3 The general process of cement three-dimensional registration

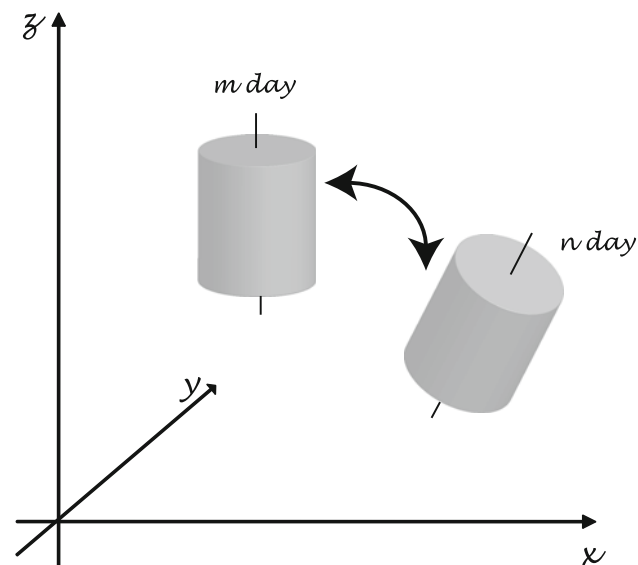


Fig. 4 The rigid transformation between cement cylinder at  $n$  day and  $m$  day,  $n \neq m$

neighbor interpolation [21] for their predominant features. This method has low time complexity, and more importantly, the distribution of gray value will not be changed.

If the point which needs interpolation is  $p$ , distance will be calculated between  $p$  and the nearest eight points in three-dimensional lattice, respectively. Gray value of  $p$ 's

nearest point which has the minimum distance will be assigned to  $p$ .

### 3.3.3 Similarity metric

To evaluate the difference between reference image and floating image, mean squared error (MSE) of gray level is used as a similarity metric in cement registration. The use of MSE leads to the assumption that point intensity is conserved between images to be registered, but at different locations. The intensity conservation assumption comes into existence approximately in this problem for the following reasons. Firstly, after the setting of cement paste, the relative positions between cement particles are fixed. Secondly, the scan parameters are fixed for each of scan to ensure the consistency of intensities. Finally, the spatial resolution leads to the particles shown in field of view are larger ones. Most of reactants in larger particles remain unhydrated in 28 days, which means the intensities in image remain unchanged.

The error is used to measure how a voxel in the reference image differs from it in the floating image. MSE measures the average of the squares of the errors. It is defined as follows:

$$MSE = \frac{\sum_{i=1}^N [g(r_i) - g(s_i)]^2}{N} \tag{3}$$

where  $N$  represents the number of voxels,  $r_i$  represents voxel  $i$  in reference image and  $s_i$  represents the same voxel in floating image.  $g(r_i)$  is the gray value of  $r_i$  and  $g(s_i)$  is the gray value of  $s_i$ .

### 3.3.4 Optimization objective

As far as the optimization objective of three-dimensional cement registration is concerned, the six degrees of freedom in rigid transformation are inputs while MSE between reference image and floating image is output. Let  $\vec{X} = \{t_x, t_y, t_z, \theta_x, \theta_y, \theta_z\}$  be the vector of combination of degrees of freedom. This can be defined as a function  $f$ .

$$f(\vec{X}) = MSE \tag{4}$$

The optimization algorithms, such as genetic algorithm (GA) [22], particle swarm optimization (PSO) [23], and Powell method (PM) [24], etc., can be used to optimize the degrees of freedom to minimize function  $f$ . Powell method, which was first proposed as a direct searching method by Powell in 1964, is adopted to optimize the six degrees of freedom for its predominant features, such as fast and no taking derivatives. It is an algorithm for searching local minimum of function and is one of the most commonly used algorithm in the registration [25–27].

## 4 Experiments and results

### 4.1 Data acquisition

Three types of Portland cement were used in our experiments and notated by A, B and C, respectively. Chemical composition, specific surface and sieve residue on 74 μ of these specimens are listed in Table 1. Weight ratios of C<sub>3</sub>S, C<sub>2</sub>S, C<sub>3</sub>A and C<sub>4</sub>AF are calculated according to the formula established by Bogue [28].

Four specimens were prepared for viewing in the microtomography. The appropriate masses of cement (typically 100 g) and water were added to a small beaker with different water-to-cement mass ratios (*w/c*) and cement types (Table 2). The paste was mixed by hand for 1 min in the beaker, followed by another 1 min of mixing using a electric mixer. The sides of the beaker were then scraped. Then, the molds were fixed on both sides using clamp and the paste injected into molds carefully by an injector with big needle (*d* = 1.6 mm) to avoid the change of *w/c*.

We acquired the specimens with cylinder shape and 4 mm diameter by curing them at 20 °C and 95 %

humidity in curing chamber for 24 hours. Then, they were continuously cured in water in narrow-mouth bottles. These specimens were viewed at 1, 2, 3, 4, 5, 6, 7, 14, 21 and 28 days using SkyScan 1172 High Resolution desktop Micro-CT System (Fig. 2). It scans the rotating small specimen, which was fixed in the center of operating platform of microtomography, with a fixed X-ray source, a Hamamatsu micro-focus tube and a CCD detector. The spot size limits the spatial resolution of the reconstructed slices to 3.5 μm in the X, Y and Z directions. Specimens were scanned at 70 kV and 100 μA. A series of projection images are recorded at different angular positions from 0 to 180 with rotation step 0.2 and exposure time 940 ms. A small number of images are also recorded to start the re-sampling of the images for fan compensation of the X-ray beam. There are 931 projection images totally. In each angular position, two-frames averaging to reduce the noise in the projection images were used. Further, flat field correction was also adopted.

A cone-beam reconstruction software NRecon was used to reconstruct the series of X-ray projection images into cross sections. The beam-hardening artifact was corrected by NRecon with the parameters array [1.0 1.0 1.0 1.0 0.3 0.0]. Besides, ring artifact was reduced by Sijbers and Postnov method. According to this method, four groups of 3D cement image were acquired. In each group, there are ten 1,280 × 1,280 × 969 3D cement images, each of which is isometric and corresponds to one age in hydration, with a voxel resolution of 3.58 μm (Fig. 5).

### 4.2 Experimental results

For each specimen, the 3D image at the second day is selected as the reference image for 3D registration. Then, the other cement images at different ages were registered using the proposed method. We employed a desktop supercomputer with Windows and C programming environment as our registration platform.

The change of cement 3D microstructure with time, i.e., the dynamic 3D microstructure, is imaged and analyzed after three-dimensional registration. Figure 6 shows the evolution of registered microstructure with hydration time from cross-section view.

In the microstructure, the brightest phases are anhydrous cement particles while the darkest phases are pores and air voids. C–S–H and undifferentiated hydration products are gray. As the age of the specimens increases, the anhydrous cement reacts to give hydrated phases that fill the pores. This is clearly observed from Figs. 6 and 7. Hydration products fill the pores and air voids gradually. It is noticeable on specimen 2 and specimen 4, both of which have higher *w/c*, i.e., 0.45. High *w/c* ensures adequate hydration reaction and produces more hydration products

**Table 1** Chemical compositions and physical properties of the cements prepared

	A	B	C
CaO (%)	63.89	63.74	64.74
SiO <sub>2</sub> (%)	22.58	20.93	20.72
Fe <sub>2</sub> O <sub>3</sub> (%)	3.03	3.77	3.74
Al <sub>2</sub> O <sub>3</sub> (%)	4.67	4.45	4.66
MgO (%)	2.46	2.51	3.34
SO <sub>3</sub> (%)	1.75	1.56	1.38
K <sub>2</sub> O (%)	1.2	0.93	0.54
Na <sub>2</sub> O (%)	0.17	0.23	0.19
fCaO (%)	0.64	1.01	1.25
C <sub>3</sub> S (%)	45.12	56.5	60.34
C <sub>2</sub> S (%)	30.79	17.47	13.97
C <sub>3</sub> A (%)	7.25	5.42	6.03
C <sub>4</sub> AF (%)	9.21	11.46	11.37
Specific surface (cm <sup>2</sup> /g)	4,088	3,475	4,397
Sieve residue on 74 μ (%)	3.56	6.44	3.63

**Table 2** The experimental parameters

Specimen	Cement	<i>w/c</i>
1	A	0.35
2	A	0.45
3	B	0.35
4	C	0.45

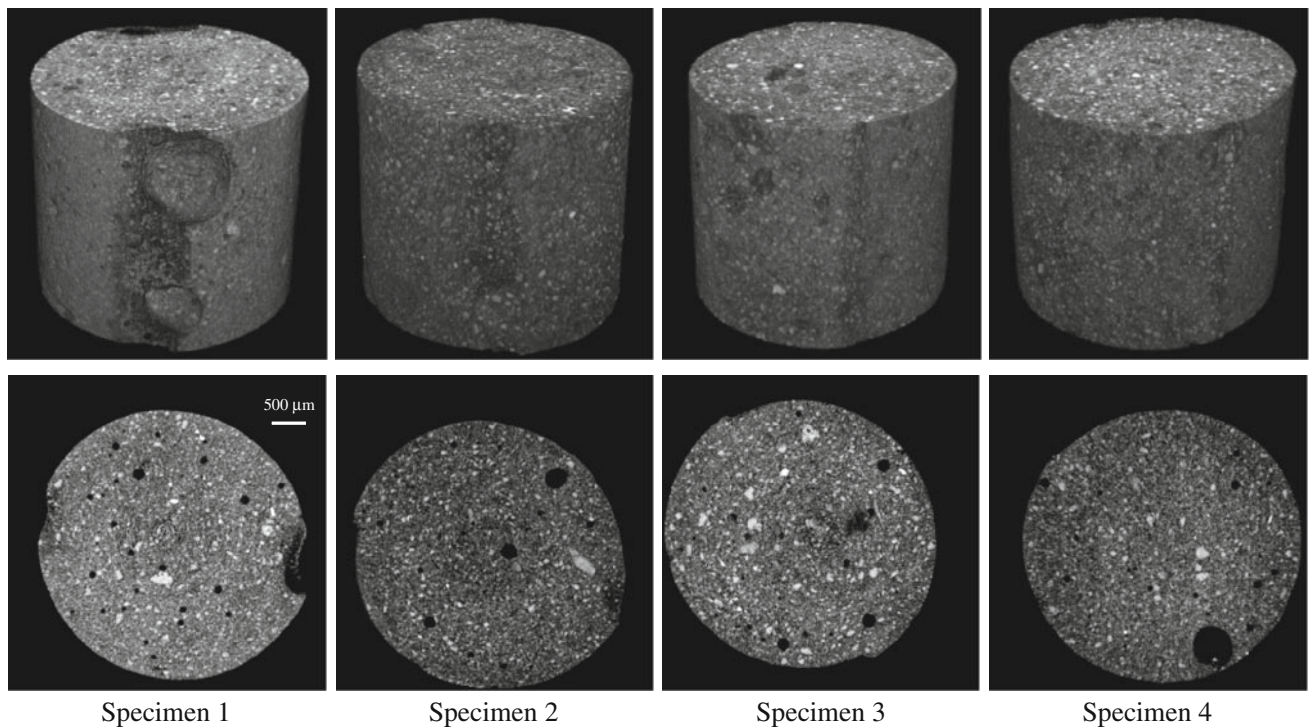


**Fig. 5** Acquired cement data at 7 days: three dimension (*top*) and cross section (*bottom*)

for filling. However, high water-to-cement ratio also leads to high porosity. The visual effect of microstructure of these two specimens looks darker because the porosity is high.

A region of interest (ROI) of volume of  $2,506 \times 2,506 \times 2,506 \mu\text{m}^3$  is taken in the center of cement cylinder. The evolution of ROI of specimen 2 and specimen 4 is shown in Fig. 8 from three-dimensional view. In this figure, one can see distinct changes of the evolution of 3D microstructure with hydration. Besides, it is widely accepted the entrained air voids play a beneficial role for the freeze-thaw durability. According to dynamic three-dimensional microstructure, the gradually filling of air void can also be shown from three-dimensional view (Fig. 9). The threshold method based on gray level histograms isolates the air voids of the pastes from the bulk. The change of air void during 28 days can be observed clearly. In addition, from the particles view, the magnified part of microstructure (Fig. 10), which is visualized by volume rendering, clearly shows the decrease and the deformation of unreacted anhydrous cement particles with the consumption of minerals in hydration.

### 4.3 Analysis

This sub-section describes the quantitative analysis of microstructural parameters on both standard deviation of

voxels value and volume fraction on the dynamic 3D microstructure. Figure 11 shows the variation of standard deviation of voxels value with evolution of hydration. The decreasing trend of standard deviation means cement microstructure becomes more homogeneous with time. The brightest anhydrous particles are consumed while the darkest pores and air voids are filled by constantly created gray hydration products. In addition, standard deviation decreases more in specimen 2 and specimen 4 from 1 to 28 days, by a margin of 3.46 and 3.47, respectively. These results verify the relation between  $w/c$  and homogeneity, high  $w/c$  speeds up the speed towards homogeneity and ensures adequate hydration.

During hydration, the volume fraction changes in water and solid phases indicate the evolution of microstructure for cement paste. Figure 12 shows the volume fractions of water ( $\frac{V_{\text{water}}}{V_{\text{solidphases}} + V_{\text{water}}}$ ) in different cement specimens at various ages. The threshold method was used to distinguish solid phase and water. We admit that the threshold method is not robust enough, but it is easy to implement than the other methods, e.g., X-ray analysis or regional growth, and is widely used for phase classification in cement microstructure. Therefore, the volume fractions are only approximation to the real volume fractions. Here the total solids volume fraction includes C–S–H, CH crystals, unhydrated cement, chemically combined water and fine pores within the particle. By comparing the volume

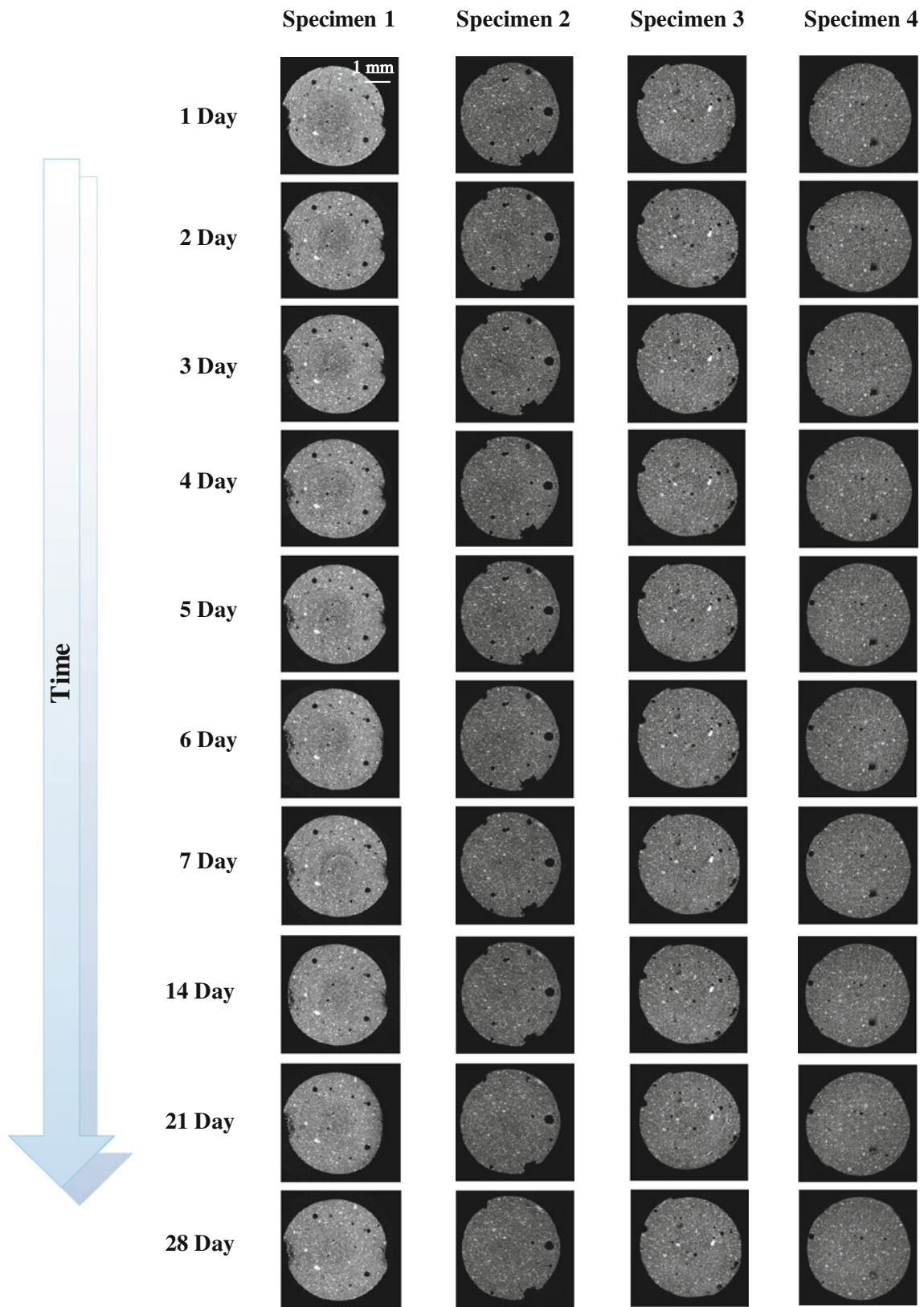


**Fig. 6** Evolution of registered microstructure with hydration time from cross-section view

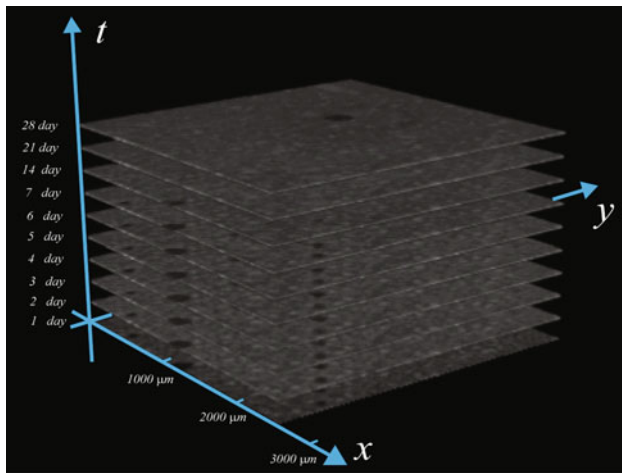


**Fig. 7** The time history of cross section. Each layer corresponds to the cross section of one age

fractions of each phase 1 and 28 days, it can be noticed that for all these specimens, the water volume is reducing. The volume of solids is increasing with the age.

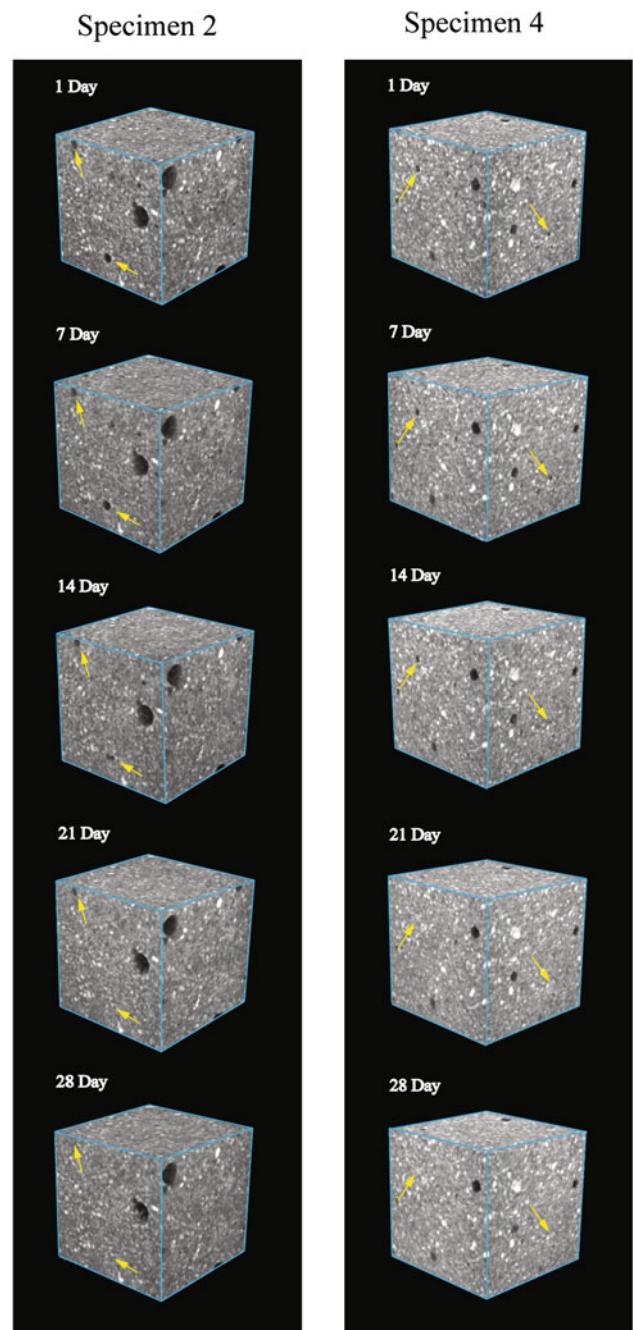
Since specimens 1 and 2 use the same cement type, the volume fractions of water change from 0.039 to 0.027 and 0.182 to 0.160 for pastes with  $w/c$  ratio 0.35 and 0.45, respectively. It can be observed from the variation that the water decrease is based on the mix proportion. For the same cement type, the higher the  $w/c$  ratio is, the higher the final volume fraction is and the larger the hydration rates is [12].

Figure 13 illustrates the comparison between the results with using registration and without using registration on specimen 1. It can be observed that the curve with using image registration is more reasonable. The small data is the lack of statistical representation, because cement paste is inhomogeneous in a small scale. This result reflects the image registration avoids the impact of position of ROI and helps us to analyze statistical parameters in the same region.

### 5 Conclusions

In this paper, an image registration based-approach is proposed to image the dynamic three-dimensional microstructure. This is the first time that the dynamic three-dimensional microstructure is imaged and analyzed for the hydration of cement.

To ensure the object fits inside the field of view and that it does not move during the scan, a couple of aluminum mold is customized to make cement specimen. The prepared specimens are scanned at different ages using microtomography. Then, the 3D images are reconstructed from X-ray projection images. Both beam-hardening artifact and ring artifact are corrected and reduced using image



**Fig. 8** Evolution of cement microstructure from three-dimensional view. The length of side is 2,506  $\mu\text{m}$

technologies. The image of dynamic microstructure of cement specimen is built by three-dimensional registration from the images of the same specimen viewed at different ages.

Evolving microstructure of cement pastes are observed clearly using the proposed approach. Further, by employing image analysis techniques on the dynamic images, quantitative analysis of microstructural parameters can also be investigated.

**Fig. 9** The gradual reduction of air void

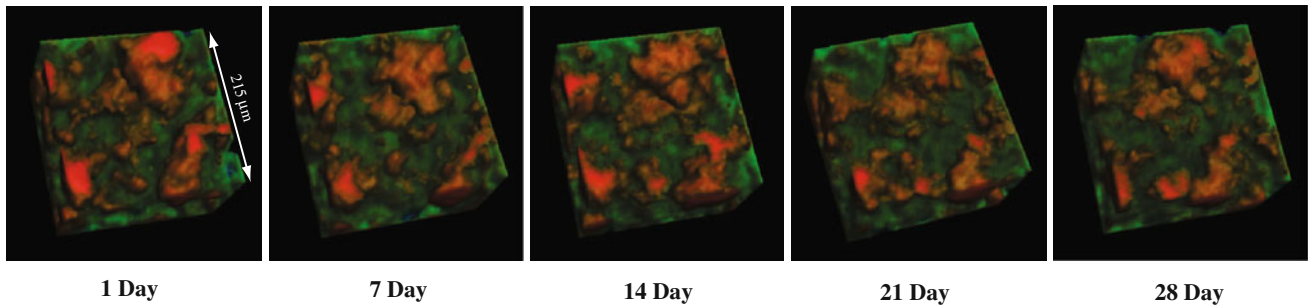
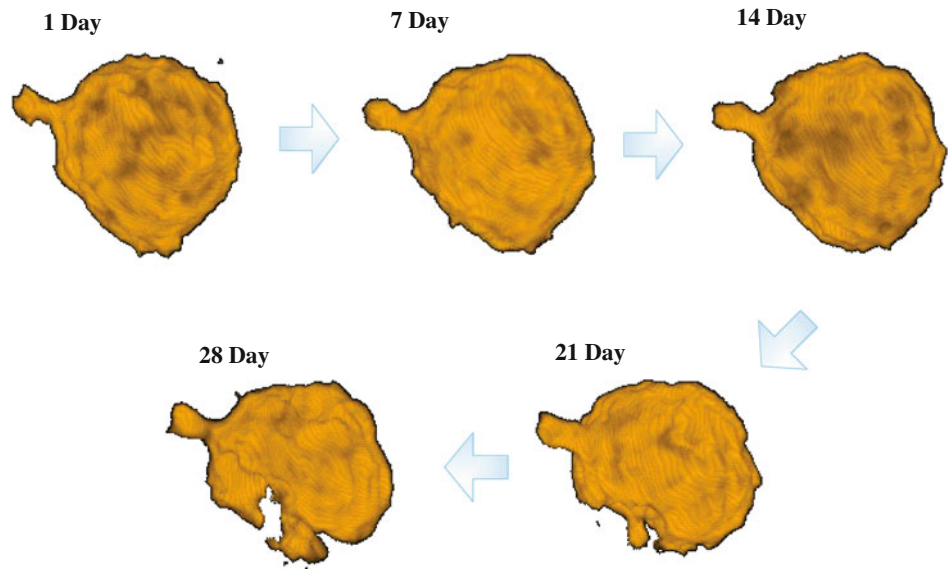


**Fig. 10** The decrease of unreacted anhydrous cement particles

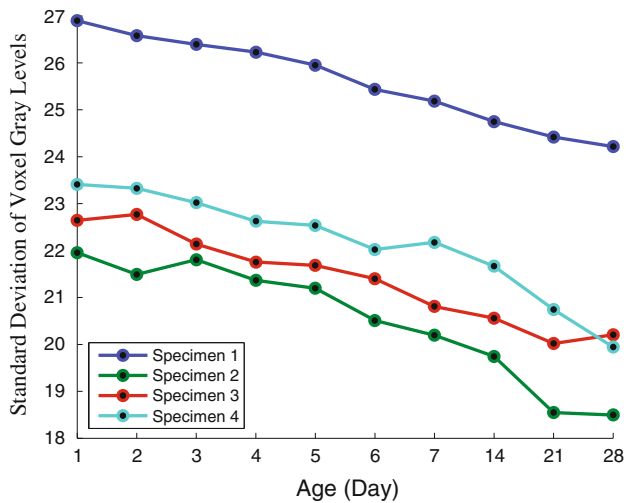


**Fig. 11** Change of standard deviation of voxel gray levels

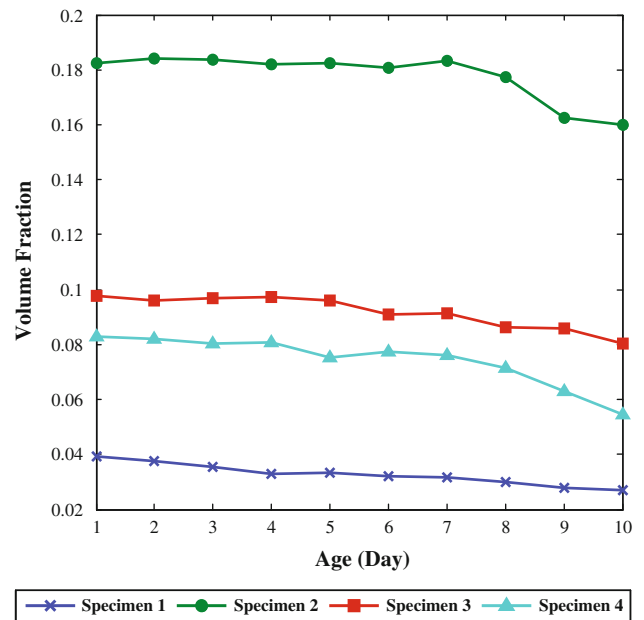


**Fig. 12** Variation of volume fraction of different cement specimens

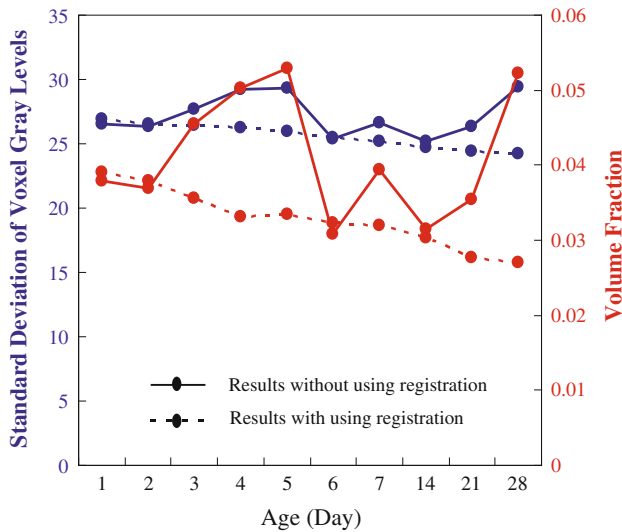


**Fig. 13** The comparison between the results with using registration and without using registration on specimen 1

Considering the complex curing condition of set cement in practice, there will be internal deformation during hydration, especially when bearing external forces. The non-rigid registration will be further studied in the future to make it much more effective in practice.

**Acknowledgments** This work was supported by National Key Technology Research and Development Program of the Ministry of Science and Technology under Grant 2012BAF12B07-3. National Natural Science Foundation of China under Grant No. 61173078, No. 61203105, No. 61173079, No. 61070130, No. 60903176. Provincial Natural Science Foundation for Outstanding Young Scholars of Shandong under Grant No. JQ200820. Shandong Provincial Natural Science Foundation, China, under Grant No. ZR2010FM047, No. ZR2012FQ016, No. ZR2012FM010. Program for New Century Excellent Talents in University under Grant No. NCET-10-0863.

**References**

1. Chen W, Brouwers HJH (2008) Mitigating the effects of system resolution on computer simulation of Portland cement hydration. *Cement Concrete Compos* 30(9):779–787
2. Thomas JJ, Biernacki JJ, Bullard JW et al (2011) Modeling and simulation of cement hydration kinetics and microstructure development. *Cement Concrete Res* 41(12):1257–1278
3. van Breugel K (1995) Numerical simulation of hydration and microstructural development in hardening cement paste (I): theory. *Cement Concrete Res* 25(2):319–331
4. Bentz DP (1997) Three-dimensional computer simulation of cement hydration and microstructure development. *J Am Ceram Soc* 80(1):3–21
5. Bullard JW (2007) A three-dimensional microstructural model of reactions and transport in aqueous mineral systems. *Model Simul Mater Sci Eng* 15(7):711–738
6. Bishnoi S, Scrivener KL (2009)  $\mu$ c: a new platform for modelling the hydration of cements. *Cement Concrete Res* 39(4): 266–274

7. Bentz DP, Mizell S, Satterfield S et al (2002) The visible cement data set. *J Res Natl Inst Stand Technol* 107(2):137–148
8. Gallucci E, Scrivener K, Grosio A et al (2007) 3D experimental investigation of the microstructure of cement pastes using synchrotron X-ray microtomography ( $\mu$ CT). *Cement Concrete Res* 37(3):360–368
9. Promentilla MAB, Sugiyama T, Shimura K (2008) Three-dimensional imaging of cement-based materials with X-ray tomographic microscopy: visualization and quantification. *Int Conf Microstruct Relat Durab Cem Compos* 61:1357–1366
10. Pourchez J, Ruot B, Debayle J, Pourchez E, Grosseau P (2010) Some aspects of cellulose ethers influence on water transport and porous structure of cement-based materials. *Cement Concrete Res* 40(2):242–252
11. Skalny J, Gebauer J, Odler I (2001) Scanning electron microscopy in concrete petrography. *Materials Scien Concrete Special Volume: Calcium Hydroxide in Concrete*, pp 59–72
12. Venkuteela G, Sun Z (2010) In situ observation of cement particle growth during setting. *Cement Concrete Compos* 32(3):211–218
13. Zitova B, Flusser J (2003) Image registration methods: a survey. *Image Visio Comput* 21(11):977–1000
14. Fowlkes CC, Luengo Hendriks CL, Keranen SVE et al (2008) A quantitative spatiotemporal atlas of gene expression in the *Drosophila* Blastoderm. *Cell (Cambridge, MA, US)* 133(2):364–374
15. Tomer R, Denes AS, Tessmar-Raible K et al (2010) Profiling by image registration reveals common origin of annelid mushroom bodies and vertebrate pallium. *Cell (Cambridge, MA, US)* 142(5):800–809
16. Grunwald D, Singer RH (2010) In vivo imaging of labelled endogenous b-actin mRNA during nucleocytoplasmic transport. *Nat Biotechnol* 467(7315):604–607
17. Wong A, Clausi DA (2007) ARRSI: automatic registration of remote-sensing images. *IEEE Trans Geosci Remote Sens* 45(5): 1483–1493
18. Ketcham RA, Carlson WD (2001) Acquisition, optimization and interpretation of X-ray computed tomographic imagery: applications to the geosciences. *Comput Geosci* 27(4):381–400
19. Herman GT (1979) Correction for beam hardening in computed tomography. *Phys Med Biol* 24(1):81–106
20. Sijbersand J, Postnov A (2004) Reduction of ring artifacts in high resolution micro-CT reconstructions. *Phys Med Biol* 49(14): 247–253
21. Lehmann TM, Gonner C, Spitzer K (1999) Survey: interpolation methods in medical image processing. *IEEE Trans Med Imaging* 18(11):1049–1075
22. Holland JH (1975) *Adaptation in natural and artificial systems*. University of Michigan Press, Ann Arbor
23. Eberhart RC, Kennedy J (1995) A new optimizer using particle swarm theory. *The 6th International Symposium on Micromachine and Human Science*, pp 39–43
24. Powell MJD (1964) An efficient method for finding the minimum of a function of several variables without calculating derivatives. *Comput J* 7(2):155–162
25. Tang M (2011) Automatic registration and fast volume reconstruction from serial histology sections. *Comput Vision Image Underst* 115(8):1112–1120
26. Wachowiak MP, Peters TM (2006) High-performance medical image registration using new optimization techniques. *IEEE Trans Inf Technol Biomed* 10(2):344–353
27. Mumcuoglu EU, Nar F, Yardimci Y et al (2006) Simultaneous surface registration of ictal and interictal SPECT and magnetic resonance images for epilepsy studies. *Nuclear Med Commun* 27(1):45–55
28. Bogue RH (1955) *The chemistry of Portland cement*. Reinhold Publishing Corporation, New York